# Stimulated Brillouin Scattering in the Time Domain at 1 $nm^{-1}$ Wave Vector

Danny Fainozzi,[1,*] Laura Foglia,[1] Nupur N. Khatu,[1,2,3] Claudio Masciovecchio,[1] Riccardo Mincigrucci,[1] Ettore Paltanin,[1] and Filippo Bencivenga[1]

[1]*Elettra-Sincrotrone Trieste, SS 14 km 163,5 in AREA Science Park, 34149 Trieste, Italy*
[2]*Department of Molecular Sciences and Nanosystems, Ca' Foscari University of Venice, Venice, Italy*
[3]*European XFEL, Holzkoppel 4, 22869 Schenefeld, Germany*

(Received 9 July 2023; accepted 27 November 2023; published 17 January 2024)

We used extreme ultraviolet (EUV) pulses to create transient gratings (TGs) with sub-100 nm spatial periodicity in a $\beta - Ga_2O_3$ single crystal. The EUV TG launches acoustic modes parallel to the sample surface, whose dynamics were revealed via backward diffraction of a third, time-delayed, EUV pulse. In addition, the sharp penetration depth of EUV light launches acoustic modes along the surface normal with a broad wave vector spectrum. The dynamics of selected modes at a wave vector tangibly larger ($\approx 1$ $nm^{-1}$) than the TG one is detected in the time domain via the interference between the backward diffracted TG signal and the stimulated Brillouin backscattering of the EUV probe. While stimulated Brillouin backscattering of an optical probe was reported in previous EUV TG experiments, its extension to shorter wavelengths can be used as a contactless experimental tool for filling the gap between the wave vector range accessible by inelastic hard x-ray and thermal neutron scattering techniques, and the one accessible through Brillouin scattering of visible and UV light.

DOI: 10.1103/PhysRevLett.132.033802

Studying thermal and vibrational dynamics in nanoscale materials is critical for advancing toward faster, more efficient, and more compact nanoelectronic devices, as well as for thermal barrier coatings [1], heat-assisted magnetic recording [2], nano-enhanced photovoltaics, and thermoelectric energy conversion, to name a few. For these applications, layer upon layer of very thin films are often used, with impurities added to tailor their function [3]. However, the complex structure of these materials makes it challenging to predict and characterise their thermoelastic properties. Material properties like elasticity, thermal conductivity, and heat capacity are mostly determined by collective lattice dynamics, which exhibit strong length-scale dependencies and can drastically differ when the spatial dimensions reduce from macroscopic to microscopic scales, i.e., to sizes comparable with the length scales of nanostructures.

An obstacle to the full description of thermoelastic responses in the tens of nm length scale was the lack of experimental techniques capable of accessing such range [4] without modifying or physically contacting the sample, which inherently complicates the experiment design and data interpretation. Collective lattice dynamics in condensed matter at wave vector $q > 1$ $nm^{-1}$ can be measured by inelastic scattering of hard x rays and thermal neutrons, while Brillouin scattering and optical transient grating (TG) can be used for $q < 0.1$ $nm^{-1}$. The intermediate $q = 0.1$–$1$ $nm^{-1}$ range (corresponding to the tens of nm length scale) is hardly accessible, despite efforts to expand the capabilities of Brillouin spectroscopy in the UV range [5] and for improving the performance of x-ray spectrometers [6]. Additionally, these spectroscopic methods are intrinsically limited by the instrumental resolution when measuring narrow lines, i.e., long dynamics. This limitation does not affect time-domain techniques, such as picosecond ultrasonics and time-domain thermoreflectance, where metal films or other nanostructures are fabricated on the sample for transducing an ultrafast optical excitation in a short wavelength thermoelastic perturbation [7,8]. However, this intrinsically modifies the sample under investigation.

Free-electron laser (FEL) sources permitted the extension of the TG approach in the extreme ultraviolet (EUV) enabling the excitation and probing of nanoscale thermoelasticity in a contactless fashion [9,10]. In this Letter, we exploit the EUV TG TIMER end station at the FERMI FEL (Trieste, Italy) [11,12] to probe acoustic modes in an Mg-doped $\beta - Ga_2O_3$ (001)-oriented bulk crystal with monoclinic structure (space group C2/m), obtained from the Czochralski method at the Leibniz-Institut für Kristallzüchtung [13]. The excellent surface quality (roughness $\approx 0.5$ nm RMS; as measured by atomic force microscopy [14]) and well-known elastic parameters made this sample suited for the present EUV TG experiment. In particular, it permitted us to demonstrate the possibility of detecting the dynamics of acoustic modes with a wavelength as short as $\approx 6$ nm via stimulated Brillouin backscattering (SBBS) of EUV light.

In a TG experiment, two time-coincident pulses of wavelength $\lambda$ (referred to as pumps) are overlapped on

 © 2024 American Physical Society

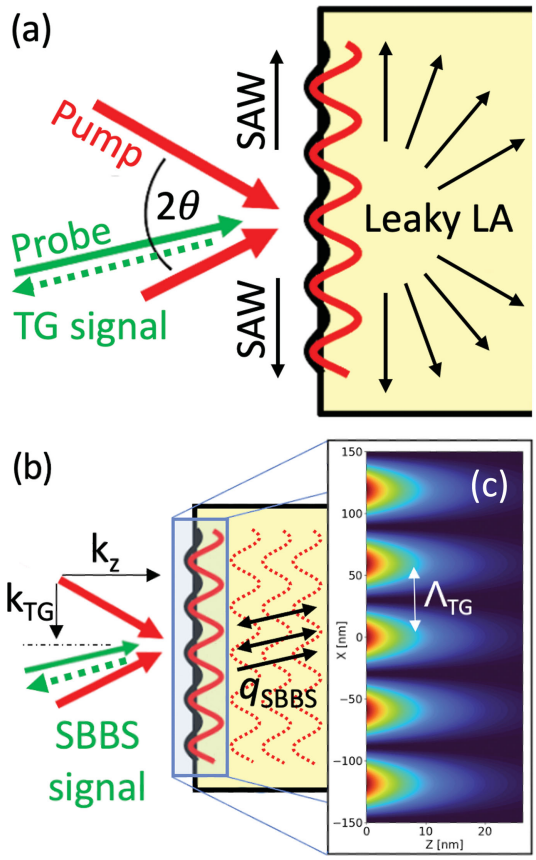


FIG. 1. (a) Schematic of the EUV TG experiment. The two crossed pulses generate an intensity grating with modulation along $q_{\mathrm{TG}}$ (parallel to the surface). This spatially periodic excitation launches surface acoustic waves (SAWs) along the surface and surface-skimming longitudinal acoustic (LA) modes in the subsurface region. These modes are probed by a time-delayed pulse in backward diffraction geometry. (b) Sketch of how the setup enables the detection of the SBBS signal along $q_{\mathrm{SBBS}}$, which is coaxial with the TG signal but generated by the intensity variation along $q_z$. (c) Simulation of the TG up to a penetration depth equal to $L_{\mathrm{abs}}^{13}$ for the 26.6/13.3 nm probe/probe configuration.

the sample at a crossing angle of $2\theta$. The interference between these two pulses induces a spatial modulation of light intensity, with period $\Lambda_{\mathrm{TG}} = \lambda/(2\sin\theta)$ and wave vector $q_{\mathrm{TG}} = 2\pi/\Lambda_{\mathrm{TG}}$; see Figs. 1(a) and 1(b). Such a patterned excitation acts as a transient diffraction grating for a third variably delayed pulse (probe), with wavelength $\lambda_{\mathrm{pr}}$, giving rise to a fourth pulse: the diffracted beam (signal).

In this experiment, two FEL pulses [time duration $\approx$ 60 fs full width at half maximum (FWHM), bandwidth $\Delta\lambda/\lambda \approx 5 \times 10^{-4}$ FWHM, repetition rate 50 Hz] are crossed on the $\beta - Ga_2O_3$ (001) sample at $2\theta = 27.6°$ (set with 2% accuracy), generating an EUV TG in the [100] direction. Two values of $\lambda$ were used: 39.9 nm and 26.6 nm, resulting in $\Lambda_{\mathrm{TG}} \approx 84$ nm and $\approx$ 56 nm, respectively. We will refer to the 39.9 nm and 26.6 nm pump-related quantities with the superscript $^{39}$ and $^{26}$, respectively. The FEL probe pulse ($\approx$ 40 fs FWHM) impinged on the sample with an angle $\theta_i = 4.6°$ with respect to the surface normal, and $\lambda_{\mathrm{pr}} =$ 13.3 nm (hereafter denoted as $^{13}$). The backward-diffracted signal beam was collected by an EUV mirror and detected by a CCD camera, as outlined in [15]. The TIMER instrument is designed to satisfy the TG phase matching conditions at the Bragg angle [i.e., $\theta_i = \theta_o = \sin^{-1}(\lambda_{\mathrm{pr}}/2\Lambda_{\mathrm{TG}})$; being $\theta_o$ the diffraction angle] for $\lambda = 3\lambda_{\mathrm{pr}}$. However, since the excitation light is absorbed in a subsurface layer shorter than $\Lambda_{\mathrm{TG}}$ [the absorption (abs) lengths of the pumps are $L_{\mathrm{abs}}^{39} \sim 12.9$ nm and $L_{\mathrm{abs}}^{26} \sim 15.9$ nm), phase matching conditions are relaxed. Therefore, only the wave vector component parallel to the sample surface ($q_{\mathrm{TG}}^{39} \approx 0.075$ nm$^{-1}$, and $q_{\mathrm{TG}}^{26} \approx 0.113$ nm$^{-1}$) is well-defined [10], while the component perpendicular to the surface ($q_z$) results in a broad spectrum, extending up to about $2\pi/L_{\mathrm{abs}}$.

Figure 1(c) further illustrates the excitation mechanism, displaying the EUV TG generated on the sample in the 26.6/13.3 configuration plotted against the $(x, z)$ coordinates, taking into account the finite value of $L_{\mathrm{abs}}^{26}$. The modulation along $x$ extends in a range much larger than the one shown in Fig. 1(c), comparable with the width (FWHM$_x$ $\approx$ hundreds of μm) of the excitation pulses. This is what we usually call TG, which launches counter-propagating acoustic waves with a wave vector equal to $\pm q_{\mathrm{TG}}$ parallel to the surface [Fig. 1(a)]. Additionally, the steep gradient along $z$ due to the finite value of $L_{\mathrm{abs}}$ launches an acoustic wave packet with a broad spectrum in $q_z$ along the $z$ direction [Fig. 1(b)]. As shown in Ref. [16], the value of $q_z = 2k\sqrt{1 - q_{\mathrm{TG}}^2/4k^2}$ satisfies the TG phase-matching conditions, yielding a backscattered signal that encodes the dynamics of SBBS modes. Here, $k = 2\pi n/\lambda_{\mathrm{pr}}$ is the wave vector of the probe in the medium, where $n$ is the refractive index at $\lambda_{\mathrm{pr}}$. Thus, the modulus of the acoustic wave vector for the SBBS signal is

$$q_{\mathrm{SBBS}} = \sqrt{q_z^2 + q_{\mathrm{TG}}^2} = 2k = \frac{4\pi n}{\lambda_{\mathrm{pr}}}, \tag{1}$$

which is independent of $q_{\mathrm{TG}}$ and is collinear with the backward diffracted signal from the TG. We note that in an excitation scheme relying on a single pump, it is impossible to select a specific acoustic wave vector along the $z$ axis. In contrast, the phase matching condition imposed by the TG [see Eq. (1)] selects a given wave vector from the broad spectrum of acoustic modes, whose dynamics is revealed in the time domain via interference with the backward-diffracted EUV TG signal. Under these experimental conditions, the combination of the sharp penetration depth of the ultrafast EUV TG pump in the material and the short wavelength EUV probe enables the excitation and selective detection of acoustic modes with a well-defined wave vector ($\Delta q_{\mathrm{SBBS}}/q_{\mathrm{SBBS}} \approx 2\Delta\lambda/\lambda \approx 10^{-3}$) as large as

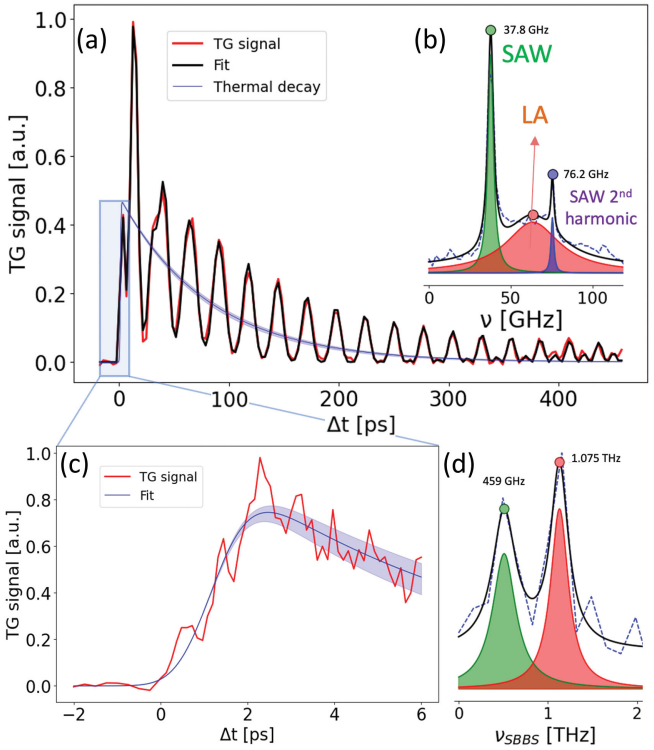


FIG. 2. (a) The long timescale dynamic of the EUV TG signal for the 39.9/13.3 nm pump/probe configuration. The slow decay is displayed in blue; the thickness of this line represents the associated error. The best fit of the signal is shown as a black line. (c) Enlargement of the first few ps, showing SBBS oscillations. The Fourier transforms, obtained after removing the slow signal variation [blue line in (a) and (c)], are reported in (b) and (d), showing respectively three modes for the long timescale and two modes for the short timescale.

$q_{\mathrm{SBBS}} \approx 1\ \mathrm{nm}^{-1}$. While stimulated Brillouin scattering is usually performed with frequency-detuned pulses matching the Brillouin frequency [17], the frequency bandwidth ($\Delta\nu > 10$ THz) of the ultrafast FEL pulses used here is sufficiently large to encompass the Brillouin shift.

Figure 2 displays the backward diffracted signal as a function of the time delay ($\Delta t$) between the EUV TG excitation and the EUV probe pulse. Measurements were conducted at both long timescales [Fig. 2(a)] and short timescales [Fig. 2(c)]. At long timescales the overall signal is characterized by a slow decay, which can be attributed to the thermal relaxation of the EUV TG [15], modulated by acoustic oscillations [9,15]; after few oscillations, the modulation becomes highly regular. For larger values of $\Delta t$, we observe double-frequency oscillations when the slow relaxation is decayed, indicating the long-living nature of this dominant mode [15]. Conversely, the irregular shape of the initial oscillations suggests the presence of additional dynamics that damp out after some tens of ps. The EUV TG data obtained at short timescales [Fig. 2(c)] were sampled with finer steps and exhibit modulations at significantly higher frequencies, compatible with the previously mentioned mixing between the SBBS signal and the backward-diffracted signal from the EUV TG.

In order to quantitatively describe the waveform at both long and short timescales an initial fitting procedure was conducted using Eq. (2):

$$I(t) = \left| \frac{1}{2}\left[1 + \mathrm{erf}\left(\frac{\Delta t}{\sigma}\right)\right] \cdot A e^{-\frac{\Delta t}{\tau}} \right|^2, \tag{2}$$

where the "erf" function accounts for a sudden rise of the signal (with $\sigma$ representing the width of the rise), followed by an exponential decay with a time constant $\tau$; results are shown as blue lines in Figs. 2(a)–2(c). Subsequently, Fourier transforms (FTs) were computed on the differences between the measured traces and their respective exponential fits. The obtained results are illustrated in Figs. 2(b)–2(d). The FTs of the long timescale waveforms present a well-defined mode and its second harmonic, plus a weaker and spectrally broader feature. The presence of this broad feature confirms the existence of a damped mode, which predominantly affects the initial portion of the waveform, as already evident from the raw data.

To describe the thermoelastic signal at long timescales, we followed the same approach as in Refs. [10,12,15,18,19], by considering the amplitude of the coherent surface displacements, whose square module is responsible for the TG signal, as the sum of the slow thermal decay and these two vibrational modes, specifically a damped sinusoidal term and a not damped one:

$$\begin{aligned} I(t) = \Bigg| \frac{1}{2}\left[1 + \mathrm{erf}\left(\frac{\Delta t}{\sigma}\right)\right] \cdot \Big[ & A e^{-\frac{\Delta t}{\tau}} \\ & - A_{\mathrm{SAW}} \sin(2\pi\nu_{\mathrm{SAW}}\Delta t + \phi_{\mathrm{SAW}}) \\ & - A_{\mathrm{LA}} \sin(2\pi\nu_{\mathrm{LA}}\Delta t + \phi_{\mathrm{LA}}) e^{-\frac{\Delta t}{\tau_{\mathrm{LA}}}} \Big] \Bigg|^2. \end{aligned} \tag{3}$$

The best-fit results are reported as a black line in Fig. 2(a). All parameters and uncertainties mentioned further below have been obtained using Eq. (3); the values extracted from the preliminary fitting with Eq. (2) and from the FTs were used as first guesses for fitting the data with Eq. (3).

The results for the oscillation frequencies are shown in Fig. 3(a) as a function of $q_{\mathrm{TG}}$. The undamped mode is compatible with a surface acoustic wave (SAW), which exhibits a linear dispersion relation vs $q_{\mathrm{TG}}$. From its slope a value for the sound velocity of $c_{\mathrm{SAW}}^{[100]} = 3.15 \pm 0.01$ km/s is obtained. This value is close to the estimated velocity of 3.24 km/s, as evaluated by using the transverse acoustic (TA) velocity $c_{\mathrm{TA}}^{[100]} = 3.57$ km/s [20] and the Poisson's ratio $\nu_p = 0.2$ [21], through the relation $c_{\mathrm{SAW}} \approx c_{\mathrm{TA}} \cdot (0.862 + 0.14\nu_p)/(1 + \nu_p)$ [22]. SAW modes represent long-living coherent surface displacements characterized by mechanical energy confined to the surface. In the employed backward-diffraction geometry, these modes are

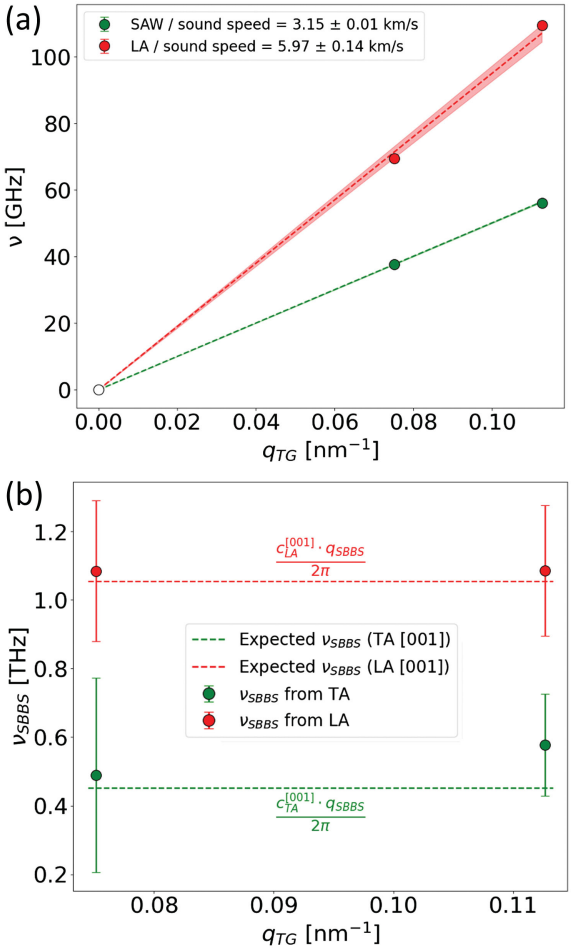


FIG. 3. The frequency of the SAW and LA modes visible in the long timescale signal are reported in (a) as a function of $q_{\mathrm{TG}}$, dashed lines indicate the slope of the linear dispersion, full lines represent the associated error. (b) SBBS frequencies; dashed lines are the values expected from the sound velocity. [20].

expected to be the dominant contribution to the EUV TG signal, as observed experimentally.

The damped mode also presents a liner dispersion with a velocity $c_{\mathrm{LA}}^{[100]} = 5.97 \pm 0.14$, which is similar to the expected value (6.18 km/s) for longitudinal acoustic (LA) modes [20]. Such marginal deviations between the expected and observed velocities may arise from factors such as slight misalignment of the sample relative to the [100] crystallographic direction, sample heating caused by the FEL, or the 10° tilt in the $(x, y)$ plane, necessary for collecting the backward-diffracted signal [11].

Surface-skimming LA modes and, more in general, bulk waves are expected in these types of TG experiments [23,24], although they do not contribute significantly in the employed geometry and are often disregarded. At these $q$ values bulk modes are not expected to show tangible damping in the probed $\Delta t$ range, while these data indicate a quite fast decay time, i.e., $\tau_{\mathrm{LA}}^{39} = 22.5 \pm 1.5$ ps and $\tau_{\mathrm{LA}}^{26} = 17.6 \pm 1.5$ ps, which is compatible with the broad feature observed in the FT [see Fig. 2(b). Though elucidating the strong damping of such modes goes beyond the scope of the present work, a possible qualitative explanation is the steep variation of the excitation intensity along the sample depth. This makes LA modes strongly influenced by the surface and they can manifest as leaky waves [24], which move away from the subsurface region toward the bulk (note that in this experiment we are observing a thin region below the surface, with thickness $\approx L_{\mathrm{abs}}^{13} = 26.3$ nm). Another aspect that may affect the decay of the LA mode is the anharmonicity due to the pump-induced temperature rise and related atomic displacement; indeed the anharmonicity of acoustic modes in $\beta - \mathrm{Ga_2O_3}$ is already tangible at room temperature [20]. Following Ref. [15] we can estimate an amplitude of surface displacement of 2 pm and, following Ref. [25], a temperature rise of ≈200 K in the uppermost 10 nm of the sample [26].

The FTs of the short timescale waveforms exhibit two main peaks [Fig. 2(d)] rising above a noisy background, located at considerably higher frequencies compared to SAW and LA modes. Furthermore, these peaks do not disperse vs $q_{\mathrm{TG}}$, as shown in Fig. 3(b). This behavior is expected from the SBBS of the EUV probe since the acoustic mode wave vector is given by $q_{\mathrm{SBBS}}$ and in this specific case the dependence on $q_{\mathrm{TG}}$ can be neglected [see Eq. (1)]. The absence of dispersion vs $q_{\mathrm{TG}}$ does not imply that SBBS modes do not exhibit dispersion; rather, it indicates that the changes in $q_{\mathrm{TG}}$ under these specific experimental conditions were not sufficient to significantly alter $q_{\mathrm{SBBS}}$. A more effective approach to modifying $q_{\mathrm{SBBS}}$ would be to vary $\lambda_{\mathrm{pr}}$, as in this case $q_{\mathrm{SBBS}} \propto \lambda_{\mathrm{pr}}^{-1}$ [see Eq. (1)].

On the other hand, the observed frequencies ($\nu_{\mathrm{SBBS}}$; as extracted from the FTs) match the ones expected by considering the sound velocities of TA ($c_{\mathrm{SAW}}^{[001]} = 4.01$ km/s) and LA ($c_{\mathrm{LA}}^{[001]} = 7.55$ km/s) modes along the relevant crystallographic direction [20]; see Fig. 3(b). Indeed, the LA mode detected via SBBS propagates along $q_{\mathrm{SBBS}}$, which means at a small tilt angle ($\phi^{39} = 4.8°$ and $\phi^{26} = 7.2°$) with respect to $q_z$, i.e., essentially toward the bulk of the sample ([001]). This is a different crystallographic direction with respect to the leaky LA mode detected at long timescales [see Fig. 2(a)], which essentially propagates beneath the surface ([100]) with wave vector $q_{\mathrm{TG}} \ll q_{\mathrm{SBBS}}$. However, since the employed setup did not allow precisely selecting crystallographic directions, all modes have to be regarded as quasi-LA and quasi-TA. It is worth mentioning that Brillouin backscattering from quasi-TA modes can be observed in monoclinic crystals, exhibiting signal amplitudes (in the optical regime) comparable to those from quasi-LA modes [27–29]. However, while EUV SBBS reasonably follows the same selection rules as optical Brillouin, the signal amplitude may differ due to wavelength-dependent

variations in the photoelastic constants, which are not known in the EUV. Indeed, studying the amplitudes of LA and TA modes in the SBBS signal as a function of the orientation of the crystal could be an approach for determining the photoelastic constants in the EUV regime. Most likely, the modes associated with larger density variations provide stronger EUV SBBS signals, as the EUV refractive index (far from core-hole resonances) primarily depends on density [12]. Further experiments are required to investigate these aspects.

The combination of the sharp penetration depth of EUV excitation pulses and the phase-matching conditions imposed by the EUV TG permitted the detection of stimulated backscattered Brillouin oscillations with a wave vector as large as $\approx 1\ \mathrm{nm}^{-1}$. This wave vector range overlaps with the lower limit of the wave vector range covered by inelastic scattering of hard x-rays and thermal neutrons. The limitations in $q_{\mathrm{SBBS}}$ mainly come from the wavelength of the probe and can be straightforwardly overcome by using a shorter probe wavelength, which can be envisioned extending all the way to the x-ray spectral range [30]. This would provide a longer penetration depth and an increased range in $q_{\mathrm{SBBS}}$.

The described approach also allowed for the detection of high-frequency surface acoustic waves and longitudinal acoustic modes propagating below the surface, without the need for nanofabrication. In fact, unlike optical laser excitation, EUV photons are highly absorbed by any material. The current setup at FERMI already makes it possible to conduct transient grating measurements at grating periods as short as 24 nm [10,31], and a further extension down to approximately 10 nm is feasible, pushing the SAW frequency close to the THz region and $q_{\mathrm{SBBS}}$ above $1\ \mathrm{nm}^{-1}$.

The authors thank Z. Galazka from Leibniz-Institut für Kristallzüchtung for providing the $\beta - Ga_2O_3$ (001) sample and Alexei Maznev (MIT, Boston) for useful discussions. E. P. acknowledges funding from the Horizon 2020 Framework Programme under the Marie Skłodowska-Curie Grant Agreement No. 860553.

*Corresponding author: danny.fainozzi@elettra.eu

[1] X. Qian, J. Zhou, and G. Chen, Phonon-engineered extreme thermal conductivity materials, Nat. Mater. **20**, 1188 (2021).

[2] T. Rausch, E. Gage, and J. Dykes, Heat assisted magnetic recording, in *Ultrafast Magnetism I: Proceedings of the International Conference UMC 2013 Strasbourg, France, 2013* (Springer, New York, 2014), pp. 200–202, 10.1007/978-3-319-07743-7_63.

[3] T. D. Frazer, J. L. Knobloch, J. N. Hernández-Charpak, K. M. Hoogeboom-Pot, D. Nardi, S. Yazdi, W. Chao, E. H. Anderson, M. K. Tripp, S. W. King *et al.*, Full characterization of ultrathin 5-nm low-*k* dielectric bilayers: Influence of dopants and surfaces on the mechanical properties, Phys. Rev. Mater. **4**, 073603 (2020).

[4] F. Bencivenga and C. Masciovecchio, Fel-based transient grating spectroscopy to investigate nanoscale dynamics, Nucl. Instrum. Methods Phys. Res., Sect. A **606**, 785 (2009).

[5] F. Bencivenga, A. Battistoni, D. Fioretto, A. Gessini, J. Sandercock, and C. Masciovecchio, A high resolution ultraviolet brillouin scattering set-up, Rev. Sci. Instrum. **83**, 103102 (2012).

[6] Y. Shvyd'ko, S. Stoupin, D. Shu, S. P. Collins, K. Mundboth, J. Sutter, and M. Tolkiehn, High-contrast sub-millivolt inelastic x-ray scattering for nano-and mesoscale science, Nat. Commun. **5**, 4219 (2014).

[7] R. Legrand, A. Huynh, B. Jusserand, B. Perrin, and A. Lemaitre, Direct measurement of coherent subterahertz acoustic phonons mean free path in GaAs, Phys. Rev. B **93**, 184304 (2016).

[8] T.-H. Chou, L. Lindsay, A. A. Maznev, J. S. Gandhi, D. W. Stokes, R. L. Forrest, A. Bensaoula, K. A. Nelson, and C.-K. Sun, Long mean free paths of room-temperature THz acoustic phonons in a high thermal conductivity material, Phys. Rev. B **100**, 094302 (2019).

[9] F. Bencivenga, R. Mincigrucci, F. Capotondi, L. Foglia, D. Naumenko, A. A. Maznev, E. Pedersoli, A. Simoncig, F. Caporaletti, V. Chiloyan *et al.*, Nanoscale transient gratings excited and probed by extreme ultraviolet femtosecond pulses, Sci. Adv. **5**, eaaw5805 (2019).

[10] L. Foglia, R. Mincigrucci, A. A. Maznev, G. Baldi, F. Capotondi, F. Caporaletti, R. Comin, D. De Angelis, R. Duncan, D. Fainozzi *et al.*, Extreme ultraviolet transient gratings: A tool for nanoscale photoacoustics, Photoacoustics **29**, 100453 (2023).

[11] R. Mincigrucci, L. Foglia, D. Naumenko, E. Pedersoli, A. Simoncig, R. Cucini, A. Gessini, M. Kiskinova, G. Kurdi, N. Mahne *et al.*, Advances in instrumentation for fel-based four-wave-mixing experiments, Nucl. Instrum. Methods Phys. Res., Sect. A **907**, 132 (2018).

[12] F. Bencivenga, F. Capotondi, L. Foglia, R. Mincigrucci, and C. Masciovecchio, Extreme ultraviolet transient gratings, Adv. Phys. **8**, 2220363 (2023).

[13] Z. Galazka, R. Uecker, D. Klimm, K. Irmscher, M. Naumann, M. Pietsch, A. Kwasniewski, R. Bertram, S. Ganschow, and M. Bickermann, Scaling-up of bulk $\beta - Ga_2O_3$ single crystals by the Czochralski method, ECS J. Solid State Sci. Technol. **6**, Q3007 (2016).

[14] As a rule of thumb, for EUV TG in reflection geometry close to normal incidence we suggest using a sample having an RMS roughness $< \lambda_{\mathrm{pr}}/10$, which is roughly equivalent to the loss of less than 1 order of magnitude in signal intensity due to the decrease in EUV reflectivity.

[15] A. A. Maznev, R. Mincigrucci, F. Bencivenga, V. Unikandanunni, F. Capotondi, G. Chen, Z. Ding, R. Duncan, L. Foglia, M. Izzo *et al.*, Generation and detection of 50 GHz surface acoustic waves by extreme ultraviolet pulses, Appl. Phys. Lett. **119**, 044102 (2021).

[16] A. A. Maznev, F. Bencivenga, A. Cannizzo, F. Capotondi, R. Cucini, R. Duncan, T. Feurer, T. Frazer, L. Foglia, H.-M. Frey *et al.*, Generation of coherent phonons by coherent

extreme ultraviolet radiation in a transient grating experiment, Appl. Phys. Lett. **113**, 221905 (2018).
[17] Z. Bai, H. Yuan, Z. Liu, P. Xu, Q. Gao, R. J. Williams, O. Kitzler, R. P. Mildren, Y. Wang, and Z. Lu, Stimulated brillouin scattering materials, experimental design and applications: A review, Opt. Mater. **75**, 626 (2018).
[18] K. A. Nelson and M. Fayer, Laser induced phonons: A probe of intermolecular interactions in molecular solids, J. Chem. Phys. **72**, 5202 (1980).
[19] A. S. Dementjev and A. Mikhailov, Electrostrictive and thermal excitation of hypersonic vibrations by nearly opposite picosecond YAG: Nd laser pulses, Sov. J. Quantum Electron. **17**, 1061 (1987).
[20] K. Mengle and E. Kioupakis, Vibrational and electron-phonon coupling properties of $\beta - Ga_2O_3$ from first-principles calculations: Impact on the mobility and breakdown field, AIP Adv. **9**, 015313 (2019).
[21] X.-Q. Zheng, H. Zhao, Z. Jia, X. Tao, and P. X.-L. Feng, Young's modulus and corresponding orientation in $\beta - Ga_2O_3$ thin films resolved by nanomechanical resonators, Appl. Phys. Lett. **119**, 013505 (2021).
[22] L. B. Freund, *Dynamic Fracture Mechanics* (Cambridge University Press, Cambridge, England, 1998), 10.1017/CBO9780511546761.
[23] K. Zoubková, P. Stoklasová, T. Grabec, P. Sedlák, and H. Seiner, Transient grating spectroscopy for complete elastic anisotropy: Beyond the measurement of surface acoustic waves, in *2021 IEEE International Ultrasonics Symposium (IUS)* (IEEE, Red Hook, 2021), pp. 1–3, 10.1109/IUS52206.2021.9593394.
[24] J. Janušonis, T. Jansma, C. Chang, Q. Liu, A. Gatilova, A. Lomonosov, V. Shalagatskyi, T. Pezeril, V. Temnov, and R. Tobey, Transient grating spectroscopy in magnetic thin films: Simultaneous detection of elastic and magnetic dynamics, Sci. Rep. **6**, 29143 (2016).
[25] A. Milloch, R. Mincigrucci, F. Capotondi, D. De Angelis, L. Foglia, G. Kurdi, D. Naumenko, E. Pedersoli, J. S. Pelli-Cresi, A. Simoncig *et al.*, Nanoscale thermoelasticity in silicon nitride membranes: Implications for thermal management, ACS Appl. Nano Mater. **4**, 10519 (2021).
[26] These estimates are made using nominal parameters, which may vary considerably from the actual ones, so they should be considered as an indication of the order of magnitude.
[27] D. Kasprowicz, S. Mielcarek, A. Trzaskowska, A. Majchrowski, E. Michalski, and M. Drozdowski, Elastic properties of $KGd(Wo_4)_2:Ho^{3+}$ single crystals studied by brillouin spectroscopy, Cryst. Res. Technol. **42**, 1370 (2007).
[28] R. Vacher and L. Boyer, Brillouin scattering: A tool for the measurement of elastic and photoelastic constants, Phys. Rev. B **6**, 639 (1972).
[29] We did not use a signal polarization analysis, which can help in selecting LA and TA modes.
[30] J. R. Rouxel, D. Fainozzi, R. Mankowsky, B. Rösner, G. Seniutinas, R. Mincigrucci, S. Catalini, L. Foglia, R. Cucini, F. Döring *et al.*, Hard x-ray transient grating spectroscopy on bismuth germanate, Nat. Photonics **15**, 499 (2021).
[31] F. Bencivenga, R. Cucini, F. Capotondi, A. Battistoni, R. Mincigrucci, E. Giangrisostomi, A. Gessini, M. Manfredda, I. Nikolov, E. Pedersoli *et al.*, Four-wave mixing experiments with extreme ultraviolet transient gratings, Nature (London) **520**, 205 (2015).